HYBRID VISION-FORCE CONTROL FOR ROBOTIC MANIPULATORS INTERACTING WITH UNKNOWN SURFACES

Antonio C. Leite, Fernando Lizarralde and Liu Hsu*

*Department of Electrical Engineering - COPPE
Federal University of Rio de Janeiro
Rio de Janeiro, Brazil

Email: [toni, fernando, liu]@coep.ufrj.br

Abstract— A control scheme based on adaptive visual servoing and direct force control is proposed for robot manipulators to perform interaction tasks on smooth surfaces. The constraint surface, as well as the parameters of the camera, are considered to be uncertain. A fixed uncalibrated camera is used for position control, while a force sensor mounted on the robot wrist is used for force regulation. A reorientation strategy is developed to keep the end-effector orthogonal to the contact surface. Experimental results are presented to illustrate the performance of the proposed scheme.

Keywords— Adaptive Control, Force Control, Robot Vision, Robotic Manipulators.

1 Introduction

Autonomy and flexibility are fundamental requirements for the robots to operate in unstructured environments, where the physical or geometrical description of the workspace is partially unknown. One way to increase the robot flexibility in practical tasks is to integrate a number of different sensors into the robot system. Cameras are useful robotic sensors since they mimic the human sense of vision and allow the robots to locate and inspect the objects without contact. On the other hand, force sensors are useful to control the contact force or to monitor the interaction forces in order to avoid damages in the robot end-effector and manipulated object. An interesting solution is to combine visual servoing and force control in a *hybrid control* scheme so that the advantages of each sensing mode are simultaneously achieved in a given interaction task.

In this framework, some hybrid controllers were designed in order to use the information from vision and force sensors to control the robot configuration (position and orientation) during the interaction. Hosoda *et. al.* [1] proposed a hybrid control algorithm that uses on-line estimators for the constraint surface geometry and the camera-robot system parameters, but the stability of the overall closed-loop system is not proven. A method employing a hybrid control based on vision and force was developed by Pichler and Jagersand [2] to estimate the constraint geometry during the manipulation task. However, an explicit solution for the orientation of the end-effector on the contact surface was not presented. Baeten and Schutter [3] proposed a hybrid control method using vision and force to execute planar contour following tasks at corners. In this approach, a sensors fusion is realized based on the combination of commanded velocities in the task frame, but the camera needs to be calibrated with respect to the robot frame. Recently, a hybrid vision and force controller was proposed by Zhao and Cheah in [4] for robot manipulators with uncertain dynamics, kinematics and constraint surface. The control algorithm is based on an adaptive law with force and gravity regressors. However, the uncertainties in the camera model were not rigorously taken into account in the theoretical analysis.

In this paper, one considers the hybrid vision and force control problem for robot manipulators using a fixed uncalibrated camera and a force sensor. A control method is proposed to combine adaptive visual servoing and direct force control in the presence of rigid smooth surfaces with unknown geometry and uncertainties in the camera parameters. The visual servoing strategy is based on a symmetrization method via factorization of the control matrix to solve the multivariable adaptive control problem. The force control strategy is based on an integral action algorithm, due to its well-known robustness with respect to the measurement time delay and capability of removing the steady-state force error.

In order to solve the interaction problem on unknown surfaces, a method is used to estimate the constraint geometry through the force and displacement measurements [5]. Moreover, a method is presented to reorientate the end-effector on the surface during the task execution through measured contact force. The orientation control uses the unit quaternion formulation that is free of singularities and computationally efficient [6]. This paper is a follow-up of [7], where only simulation results were included. Here, experimental results are presented to illustrate the practical performance and viability of the proposed scheme.

2 Kinematic Control

In this section, one considers the kinematic control problem. Here, one assumes that: (A1) the robot kinematics is *known*; (A2) the robot dynamics is *negligible*. This last assumption is applied to most commercial robots with high gear ratios and/or when the task motions are not so fast.

Let $x = [x_1 \;\; x_2 \;\; x_3]^T$ be the position of the arm tip and $q = [q_s \;\; q_v^T]^T$ be the unit quaternion representation for the end-effector orientation, where $q_s \in \mathbb{R}$ and $q_v \in \mathbb{R}^3$ are the scalar and vectorial part of the unit quaternion respectively. In this context, the end-effector configuration $r = [x \;\; q]^T \in \mathbb{R}^m$ is given by the forward kinematics map $r = k(\theta)$, where $\theta \in \mathbb{R}^n$ is the manipulator joint angle vector.

The differential kinematics equation can be obtained as the time derivative of the forward kinematics

given by

$$\dot{r} = \begin{bmatrix} \dot{x} \\ \dot{q} \end{bmatrix} = J_k(\theta)\,\dot{\theta}\,, \tag{1}$$

where $J_k(\theta) = \frac{\partial k(\theta)}{\partial \theta} \in \mathbb{R}^{m\times n}$ is the analytical Jacobian. The end-effector velocity $v = [\dot{x}\ \ \omega]^T$, composed by the linear velocity $\dot{x}$ and the angular velocity ω, is related to $\dot{r}$ by

$$v = \begin{bmatrix} \dot{x} \\ \omega \end{bmatrix} = \begin{bmatrix} I & 0 \\ 0 & 2J_q(q) \end{bmatrix} \begin{bmatrix} \dot{x} \\ \dot{q} \end{bmatrix} = J_r\,\dot{r}\,, \tag{2}$$

where $J_q(q) = [\,-q_v \ \ \ q_s I + (q_v\times)\,]$ and J_r is the representation Jacobian. Then, substituting (1) in (2) gives

$$v = J_r\,J_k\,\dot{\theta} = J\,\dot{\theta}\,, \tag{3}$$

where $J \in \mathbb{R}^{n\times n}$ is the manipulator Jacobian. Thus, from (3) and considering $\dot{\theta}_i$ as the control input u_i ($i = 1, ..., n$) one obtains the following control system: $v = J(\theta)\,u$. A cartesian control law v_c can be transformed to joint control signals by using

$$u = J^{-1}(\theta)\,v_c = J^{-1}(\theta) \begin{bmatrix} v_p \\ v_q \end{bmatrix}, \tag{4}$$

provided that v_c does not drive the robot to *singular configurations*. Therefore, from (3) and (4) one has that $v_p = \dot{x}$ and $v_q = \omega$. Note that, v_p and v_q are designed to control the end-effector position and orientation respectively.

2.1 Position Control

Consider the control problem of tracking the desired time-varying reference $x_d(t)$ from the actual position x. Then, the control goal is given by

$$x \to x_d(t)\,, \qquad e_p = x_d - x \to 0\,, \tag{5}$$

where e_p is the position error. Thus, considering a feedforward and proportional control law given by $v_p = \dot{x}_d + K_p\,e_p$ one has that the position error dynamics is governed by $\dot{e}_p + K_p\,e_p = 0$. Hence, by a proper choice of K_p as a positive definite matrix, $e_p \to 0$ exponentially as $t \to \infty$.

2.2 Orientation Control

Consider the control problem of driving the attitude matrix R to a desired time-varying attitude $R_d(t)$. Then, the control goal is given by

$$R \to R_d(t)\,, \qquad R_\phi = R^T\,R_d \to I\,, \tag{6}$$

where R_ϕ is the error attitude matrix. Let $e_q = [e_{qs}\ \ e_{qv}^T]^T$ be the unit quaternion representation for $R_\phi \in SO(3)$ and $\dot{e}_q = \frac{1}{2} J_q^T(e_q)\,\tilde{\omega}$ be the error propagation equation [8], where $\tilde{\omega} = (\omega_d - \omega)$ and ω_d is the desired angular velocity. From the unit quaternion formulation $e_q = [1\ \ 0]^T$ if and only if R and R_d are aligned.

The control design uses the Lyapunov function candidate given by $2V = (e_{qs} - 1)^2 + e_{qv}^T\,e_{qv}$. Differentiating V with respect to time along the system trajectories one has that $\dot{V} = -e_{qv}^T\,\tilde{\omega}$. Thus, setting $\tilde{\omega} = K_o\,e_{qv}$ and considering K_o as a positive definite matrix, implies that $\dot{V}$ is negative semidefinite. Then, the orientation control law has the form

$$v_q = \omega_d + K_o\,e_{qv}\,. \tag{7}$$

Since V is continuously differentiable, radially unbounded, positive definite and $\dot{V} \le 0$ over the entire state space, by using the *LaSalle's theorem* [9] one has that all system trajectories converge to the largest invariant set $\bar{\Omega}$ in $\Omega = \{(e_{qs}\,, e_{qv}) : \dot{V} = 0\} = \{(e_{qs}\,, e_{qv}) : e_{qv} = 0\}$. In the invariant set one has that $\tilde{\omega} = 0$ and thus $\dot{e}_q = 0$. The constraint $e_{qs}^2 + e_{qv}^2 = 1$ implies that $\bar{\Omega} = \{(e_{qs}\,, e_{qv}) : e_{qs} = 1\,, e_{qv} = 0\}$ and hence $(e_{qs}\,, e_{qv}) = (\pm 1\,, 0)$ is a globally asymptotically stable equilibrium.

2.3 Force Control

Consider the force control problem for a kinematic robot. Here, one assumes that the control goal is to regulate the measured contact force f to a desired force f_d along the normal vector of the constraint surface, that is,

$$f \to f_d(t)\,, \qquad e_f = f_d - f \to 0\,, \tag{8}$$

where e_f is the force error. Similar to *Hooke's law* the contact force can be modeled by $f = -k_s\,(x_3 - l_s)$, where k_s is the spring elastic constant and l_s is the spring free length. Then, using a PI control law

$$v_f = k_p\,e_f + k_i \int_0^t e_f(\tau)\,d\tau\,, \tag{9}$$

one has that the force error dynamics is governed by $\ddot{e}_f + k_s\,k_p\,\dot{e}_f + k_s\,k_i\,e_f = 0$, where k_p and k_i are the feedback gains. Hence, by a proper choice of k_p and k_i as positive constants, $e_f \to 0$ exponentially as $t \to \infty$.

3 Hybrid Control Scheme

The hybrid force and position control combines the force and moment information with position or velocity data according to *Mason's concept* [10] that defines two complementary orthogonal subspaces in force and movement. Thus, the force and position constraints can be separately considered and the controllers are not affected by mutual interferences. These constraints are specified in a proper coordinate system for the task execution called the *constraint frame* and denoted by $\bar{E}_s$.

From the selection matrices $S \in \mathbb{R}^{3\times 3}$ and $I - S$, which determine what degrees of freedom must be controlled by force and movement, the control signals are decoupled and the control laws for each subspace can be independently designed in order to achieve simultaneously different force and position requirements for a given task. Thus, the hybrid control law is given by

$$v_h = v_{hf} + v_{hp}\,, \tag{10}$$

where v_{hf} and v_{hp} are the decoupled control signals acting respectively in the force and position subspaces, such that

$$v_{hf} = R_{es}\,S\,R_{es}^T\,v_f\,, \qquad v_{hp} = R_{es}\,(I - S)\,R_{es}^T\,v_p\,.$$

Now, considering that the constraint surface in the task space can be described by $\Phi(x) = 0$, the constrained motion of the end-effector on the surface satisfies $D\,\dot{x} = 0$, where $D = \frac{\partial \Phi}{\partial x}$ denotes the *normal vector* of the surface. Thus, when the constraint geometry is *known* the rotation matrix of the constraint frame with respect to the tool frame, denoted by R_{es}, can be easily calculated.

4 Unknown Constraint Surface

Assuming that the manipulator interacts with unknown contact surfaces, it is appropriate to present a method to estimate the *geometric parameters* [6] of the constraint and update the end-effector orientation on the surface during the task execution.

4.1 Estimation of Constraint Geometry

In the hybrid control scheme one has to separate the interaction control and motion control actions along complementary directions of the task space. However, to achieve this aim in an unstructured workspace one has to find the geometry of the constraint surface and its relationship with the frames of interest. Thus, the decoupling of control variables can be executed in the constraint space, where the task is naturally described and the selection matrices have a diagonal form with 0 and 1 elements.

Then, one considers $\bar{E}_s = [\vec{e}_1 \;\; \vec{e}_2 \;\; \vec{e}_3]$ a fixed orthonormal frame in a contact point on the constraint surface where $\vec{e}_i$ $(i = 1, 2)$ defines a tangent plane to the surface. For a *frictionless* point contact the direction of the contact force is normal to the surface. Thus, based on the contact force $\vec{f}$ which is exerted by end-effector on the surface, one defines $\vec{e}_3 = \vec{f} \,/\, \|\vec{f}\|$ as an estimated normal vector of the constraint surface.

Let $\vec{\Delta x}$ be the end-effector displacement on the constraint surface during the interaction, one defines $\vec{e}_1 = \vec{\Delta x} \,/\, \|\vec{\Delta x}\|$ as an estimated tangent vector along the end-effector trajectory described on the surface. Finally, since $\vec{e}_1$ and $\vec{e}_3$ are orthonormal vectors, the vector $\vec{e}_2$ can be obtained from right-hand rule, that is, $\vec{e}_2 = \vec{e}_3 \times \vec{e}_1$.

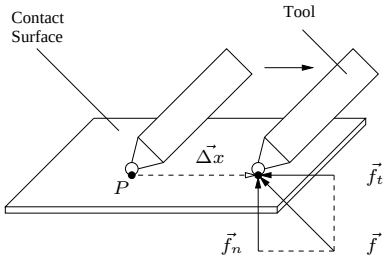

Figure 1: Tangential and normal forces in a contact point on the surface.

However, when a *frictional* surface is considered, the contact force $\vec{f}$ has a tangential component (Fig. 1). Here, one assumes that the only action of tangential forces is due to the *friction force* and it acts in the opposed direction of the end-effector displacements. Then, the estimated normal vector of the surface can be rewritten as $\vec{e}_3 = (\vec{f} - \vec{f}_t) \,/\, \|\vec{f} - \vec{f}_t\|$, and the tangential force, aligned with the movement direction, is given by $\vec{f}_t = (\vec{f} \cdot \vec{\Delta x})\, \vec{e}_1$. Hence, the constraint frame $\bar{E}_s$ can be expressed as

$$\bar{E}_s = \left[\frac{\vec{\Delta x}}{\|\vec{\Delta x}\|} \;\; \frac{\vec{f} - (\vec{f}\cdot\vec{\Delta x})\frac{\vec{\Delta x}}{\|\vec{\Delta x}\|}}{\|\vec{f} - (\vec{f}\cdot\vec{\Delta x})\frac{\vec{\Delta x}}{\|\vec{\Delta x}\|}\|} \times \frac{\vec{\Delta x}}{\|\vec{\Delta x}\|} \;\; \frac{\vec{f} - (\vec{f}\cdot\vec{\Delta x})\frac{\vec{\Delta x}}{\|\vec{\Delta x}\|}}{\|\vec{f} - (\vec{f}\cdot\vec{\Delta x})\frac{\vec{\Delta x}}{\|\vec{\Delta x}\|}\|} \right]$$

and the estimated orientation of the constraint frame $\bar{E}_s$ with respect to the tool frame $\bar{E}_e$ is given by

$$\hat{R}_{es} \;=\; [\,(\vec{e}_1)_e \;\; (\vec{e}_2)_e \;\; (\vec{e}_3)_e\,]\,. \qquad (11)$$

4.2 End-effector Reorientation

Let $f = [f_1 \;\; f_2 \;\; f_3]^T \in \mathbb{R}^3$ be the components of the contact force $\vec{f}$ exerted on the end-effector at a contact point P on an unknown surface. Here, one considers a point contact with *friction* and assumes that the contact force is exerted in any direction within the *friction cone* [6]. Therefore, contact loss or sliding on the surface are precluded.

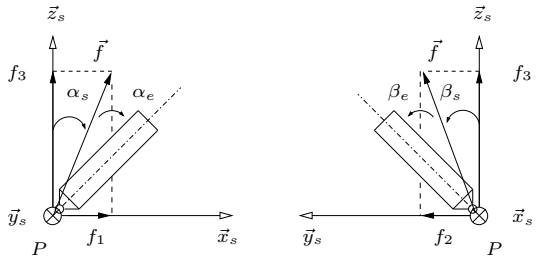

Figure 2: Force components represented in the constraint frame.

Let α_s and β_s denote the angular deviations of the contact force $\vec{f}$ with respect to the surface normal defined as

$$\alpha_s = atan\,(\,f_1\,/\,f_3\,)\,, \quad \beta_s = atan\,(\,f_2\,/\,f_3\,)\,. \qquad (12)$$

Now, let α_e and β_e denote the angular deviations between the end-effector *approach*-axis with respect to the contact force analogously defined, as shown in Figure 2. Note that, α_e and β_e are measurable from the force sensor and that α_s and β_s can be obtained by using (11). Then, to reorientate the end-effector along the axis $\vec{z}_s$ of the constraint frame, it is necessary to cancel the *deviation angles* through the following elementary rotations

$$R_\alpha = R_{y_s}\,(\alpha)\,, \quad R_\beta = R_{x_s}\,(-\beta)\,, \qquad (13)$$

where $\alpha = (\alpha_s + \alpha_e)$ and $\beta = (\beta_s + \beta_e)$. The resulting rotation matrix is given by $R_o = R_\alpha\, R_\beta$ and the desired orientation can be obtained by $R_d = R_{be}\, R_o$, where R_{be} is the rotation matrix of the tool frame with respect to the base frame.

5 Visual Servoing

In this work, one uses the visual servoing to provide closed-loop position control for the robot end-effector. Let $y = [y_1 \;\; y_2]^T$ be the end-effector position in the image frame and y_d be the desired trajectory for a target feature fixed on the arm tip. Then, the control goal can be described by

$$y \to y_d(t)\,, \qquad e_v = y_d - y \to 0\,, \qquad (14)$$

where e_v is the image error. Here, one considers a nonredundant planar manipulator, that is, $m = n = 2$ and hence the end-effector position in the robot frame is given by $x = [x_1 \;\; x_2]^T$. Then, considering a monocular fixed CCD camera with optical axis *nonperpendicular* to the robot workspace, the camera/workspace transformation can be represented by [11]

$$y = K_v(x)\, x + r_0\,, \qquad (15)$$

with

$$K_v(x) = \frac{f_0}{f_0 + z(x)} \begin{bmatrix} -\alpha_1 & 0 \\ 0 & -\alpha_2 \end{bmatrix} \begin{bmatrix} cos(\phi) & -sin(\phi) \\ sin(\phi) & cos(\phi) \end{bmatrix},$$

where r_0 is a constant term, which depends on the position of the camera frame with respect to the robot frame, K_v is the *high frequency gain matrix* and considers the camera orientation angle ϕ with respect to the robot frame, f_0 is the camera focal length, $z(x)$ is the depth from the camera plane to the robot workspace (in general $z(x) \gg f_0$), and $\alpha_i > 0$ $(i = 1, 2)$ are the scaling factors (pixels/mm).

5.1 Virtual Surface

Consider the visual servoing problem for a robot manipulator moving along a desired trajectory specified on a virtual surface in the workspace. Then, a generic 3D surface can be described by $z(x) = z_0 + F(x, \nu)$, where z_0 is a constant depth between the camera plane and robot workspace; ν is a vector of constant parameters. Without loss of generality this work limits to the case of *locally flat* surfaces given by

$$z(x) = z_0 + \epsilon\,(c^T x), \tag{16}$$

where $c = [a \;\; b]^T$ and $a, b \in \mathbb{R}$ are parameters relative to the surface slope with respect to the axes $\vec{x}_c$ and $\vec{y}_c$ in the camera frame; ϵ is a sufficiently small parameter relative to the *depth variation* in the robot workspace.

5.2 Control Problem

In this work, the cartesian control problem in the image frame is described by

$$\dot{y} = G(x)\, v_v, \tag{17}$$

where $v_v = [v_1 \;\; v_2]^T$ and $G(x)$ is an *uncertain matrix* obtained from partial derivative of $K_v(x) = [\, k_1(x) \;\; k_2(x) \,]$, that is,

$$G(x) = K_v(x) + \frac{\partial k_1(x)}{\partial x}\, x_1 + \frac{\partial k_2(x)}{\partial x}\, x_2 \tag{18}$$

and

$$\begin{aligned}
g_{11}(x) &= \frac{\alpha_1 f_0}{\Delta z^2} \left[\Delta z\, cos(\phi) + \frac{\partial z(x)}{\partial x_1}\, h_1(x) \right], \\
g_{12}(x) &= \frac{\alpha_1 f_0}{\Delta z^2} \left[-\Delta z\, sin(\phi) + \frac{\partial z(x)}{\partial x_2}\, h_1(x) \right], \\
g_{21}(x) &= \frac{\alpha_2 f_0}{\Delta z^2} \left[\Delta z\, sin(\phi) + \frac{\partial z(x)}{\partial x_1}\, h_2(x) \right], \\
g_{22}(x) &= \frac{\alpha_2 f_0}{\Delta z^2} \left[\Delta z\, cos(\phi) + \frac{\partial z(x)}{\partial x_2}\, h_2(x) \right],
\end{aligned}$$

with $\Delta z = f_0 + z(x)$, $h_1(x) = x_1 cos(\phi) - x_2 sin(\phi)$ and $h_2(x) = x_1 sin(\phi) + x_2 cos(\phi)$. In order to simplify the notation, the term x will be removed from $G(x)$. Thus, $G(x) = G = [\, g_{ij} \,]$ for $i, j = 1, 2$.

5.3 Visual-Servoing MRAC

In the model reference adaptive control approach the model can be specified by

$$\dot{y}_d = -\Lambda y_d + \Lambda y_r, \tag{19}$$

where $y_r \in \mathbb{R}^2$ is the reference signal assumed uniformly bounded $\forall t$ and $y_d \in \mathbb{R}^2$ is the desired trajectory of the end-effector in the image plane. For the sake of simplicity, one considers $\Lambda = \lambda I$. One can easily modify the algorithm presented in [12] to introduce the image error directly into the control law, even if the adaptation is frozen.

From (17) and (19), it follows that the ideal control law is given by [1]

$$v^* = \lambda G^{-1}\,(y_r - y). \tag{20}$$

Then, from image error $e_v = y_d - y$, one obtains the following error system $\dot{e}_v = -\lambda e_v - G\, v_v + \lambda(y_r - y)$, that is

$$\dot{e}_v = -\lambda e_v + G\, \tilde{v}, \tag{21}$$

where $\tilde{v} = v^* - v_v$ and $G = [g_{ij}]$ for $i, j = 1, 2$.

5.4 Adaptation via SDU factorization

From the expression of v^*, one verifies that the usual parameterization for the adaptive law would be

$$v_v = P_\Phi\,(y_r - y), \tag{22}$$

with $P_\Phi \in \mathbb{R}^{2\times 2}$ being the matrix of adaptive parameters. However, as shown in [12], this leads to crucial limitations about the prior assumptions on G, not applicable to the present problem (even when G is a constant matrix). One possible solution is to use the SDU factorization method proposed in [13]. This method is based on the factorization $G = S_v\, D_v\, U_v$, where S_v, D_v, U_v are respectively symmetric, diagonal and upper triangular matrices. If $g_{11} > 0$ and $\det(G) > 0$, then U_v (and U_v^{-1}) can be chosen with unitary diagonal elements and $D_v = I$. Thus, it can be concluded that there exists an upper triangular matrix $T = U_v^{-1}$ such that $(GT) = (GT)^T = S_v > 0$ [14]. Then, one can rewrite (21) as

$$\dot{e}_v = -\lambda e_v - S_v\,[T^{-1}\, v_v - \lambda S_v^{-1}\,(y_r - y)].$$

Thus, the ideal control law is given by

$$\begin{aligned}
v_1^* &= t_{12}\, v_2 + \lambda\, det(G^{-1})\,(s_{22}\,\rho_{v1} - g_{21}\,\rho_{v2}) \quad (23)\\
v_2^* &= -\lambda\, det(G^{-1})\,(g_{21}\,\rho_{v1} - g_{11}\,\rho_{v2}), \quad (24)
\end{aligned}$$

where $t_{12} = (g_{21} - g_{12})/g_{11}$, $s_{22} = (g_{21}^2 + det(G))/g_{11}$ and $\rho_{vi} = y_{ri} - y_i$ $(i = 1, 2)$. Note that, it is not possible to get linear parameterization for the laws (23) and (24), since v_1^* and v_2^* involve the inverse of G. However, one can use *Taylor series* approximation based on assumption that the robot movements in the workspace satisfy the condition $|z_0| > \epsilon\,|c^T x|$. Thus, one can neglect the high order terms from ϵ^2 in the series expansion. Hence, the control signal can be parameterized as

$$v_1 = \Theta_1^T w_1, \quad v_2 = \Theta_2^T w_2, \tag{25}$$

where Θ_1 and Θ_2 are the parameters vectors; w_1 and w_2 are the regressors vectors given by

$$w_1 = [v_2 \;\; \rho_{v1} \;\; \rho_{v2} \;\; v_2\, y_1 \;\; v_2\, y_2 \;\; \rho_{v1}\, y_1 \;\; \rho_{v1}\, y_2 \;\; \rho_{v2}\, y_1 \;\; \rho_{v2}\, y_2],$$
$$w_2 = [\rho_{v1} \;\; \rho_{v2} \;\; \rho_{v1}\, y_1 \;\; \rho_{v2}\, y_2 \;\; \rho_{v2}\, y_1 \;\; \rho_{v2}\, y_2],$$

[1] Note that, the equations (4) and (15)-(20) can be expressed as a resolved-rate motion control law. Substituting y_r from (19) into (20) gives $v^* = G^{-1}[\dot{y}_d + \lambda(y_d - y)]$. Then, from (4), one has that $u = (GJ(\theta))^{-1}[\dot{y}_d + \lambda(y_d - y)]$, where $J_v = GJ(\theta)$ is the image Jacobian [11].

and with $\tilde{v}^T = [\tilde{\Theta}_1^T w_1 \;\; \tilde{\Theta}_2^T w_2]$ one has that

$$\dot{e}_v = -\lambda e_v + S_v \, \tilde{v} \, ,$$

where $\tilde{\Theta}_i = \Theta_i - \Theta_i^*$ for $i = 1, 2$. From the analysis of the error dynamics, the adaptation laws for $\tilde{\Theta}_1$ and $\tilde{\Theta}_2$ are given by

$$\dot{\tilde{\Theta}}_1 = \dot{\Theta}_1 = -\gamma_1 \, e_{v1} \, w_1 \, , \quad \dot{\tilde{\Theta}}_2 = \dot{\Theta}_2 = -\gamma_2 \, e_{v2} \, w_2 \, . \quad (26)$$

5.5 Stability Analysis

Since S_v is state dependent, one assumes that: (A3) $P \triangleq S_v^{-1}$ satisfies $\frac{1}{2}\dot{P} - \lambda P < \lambda_0 I$ for some positive λ_0. Then, the gradient law $\dot{\Theta}_i$ $(i = 1, 2)$ makes the derivative of the Lyapunov function candidate $2V = e_v^T \, S_v^{-1} \, e_v + \gamma^{-1}(\tilde{\Theta}_1^T \tilde{\Theta}_1 + \tilde{\Theta}_2^T \tilde{\Theta}_2)$ negative semidefinite, since $\dot{V} = -\lambda_0 \, e_v^T \, e_v \leq 0$.

Thus, $\tilde{\Theta}_i$ and e_v are uniformly bounded and consequently $\dot{e}_v$ is uniformly bounded. Applying the usual argument based on *Barbalat's lemma* [9], one concludes that $e_v \in \mathcal{L}_2 \cap \mathcal{L}_\infty$ and $e_v(t) \to 0$ as $t \to \infty$, which proves global stability and asymptotic convergence of the tracking error.

6 Hybrid Vision-Force Control

For the hybrid vision and force control problem, a cartesian control law can be transformed to joint control signals by using

$$u = J^{-1}(\theta) \, v_c = J^{-1}(\theta) \begin{bmatrix} v_h \\ v_q \end{bmatrix} , \quad (27)$$

where v_h is given by (10) and

$$v_{hf} = \hat{R}_{es} \, S \, \hat{R}_{es}^T \, v_f \, , \qquad v_{hp} = \hat{R}_{es} \, (I - S) \, \hat{R}_{es}^T \, v_v \, .$$

The closed-loop stability analysis uses the Lyapunov function candidate given by

$$2V = e_f^T \, k_f \, k_s \, k_i \, e_f + \dot{e}_f^T \, k_f \, \dot{e}_f + (e_{qs} - 1)^2 + e_{qv}^T \, e_{qv} + e_v^T \, S_v^{-1} \, e_v + \gamma^{-1} \, (\tilde{\Theta}_1^T \tilde{\Theta}_1 + \tilde{\Theta}_2^T \tilde{\Theta}_2) \, .$$

From (A3), the time derivative of V along the trajectories of the closed-loop system is negative semidefinite, that is,

$$\dot{V} = -\dot{e}_f^T \, k_f \, k_s \, k_p \, \dot{e}_f - e_{qv}^T \, K_o \, e_{qv} - \lambda_0 \, e_v^T \, e_v \leq 0 \, .$$

Thus, e_f, $\dot{e}_f$, e_{qs}, e_{qv}, $\tilde{\Theta}_i$ and e_v are uniformly bounded and consequently $\ddot{e}_f$, $\dot{e}_{qv}$ and $\dot{e}_v$ are uniformly bounded. Applying the usual argument based on *Barbalat's lemma* [9], one concludes that $e_f \to 0$, $e_{qv} \to 0$ and $e_v \to 0$ as $t \to \infty$, which proves the global stability of the overall system.

7 Experimental Results

This section describes some preliminary experimental results obtained by implementing the proposed hybrid controller on a 6-DOF Zebra Zero robot manipulator (Integrated Motions, Inc.). The robot task involves the visual tracking of the target feature, while the end-effector tip exerts a controlled contact force on an unknown planar surface. The tool consists of a rigid cylinder coupled to the robot wrist by means of a linear spring with elastic constant given by $k_s = 640$ [N/m], aligned with the cylinder axis. This avoids hard impacts that could damage the JR3 force-torque sensor (JR3, Inc.) or the contact surface during the interaction. A KP-D50 CCD camera (Hitachi, Ltd.) with a lens of length $f_0 = 6$ [mm] was mounted in front of the Zebra Zero. The extracted visual feature is the centroid coordinates of a red disc fixed on the arm tip. The images of 640×480 [pixel] are acquired using a Meteor frame-grabber (Matrox, Ltd.) at 30 frames per second (FPS). The RGB image processing is performed on a subwindow 100×100 [pixel] wide. The first estimation of the centroid coordinates is performed off-line using image subtraction.

In this preliminary experimental test, the visual servoing loop was designed to perform the tracking of a trajectory (straight-line) with 100 [pixel] length. specified on the image plane, while the force control loop regulates the contact force to 0.6 [kgf] along the end-effector *approach*-axis. The contact surface was the outer side of a wood plane. Thus, the experiment also serves to evaluate the reorientation of the end-effector during the task execution. Figure 3 describes the time history of the image error, force error and norm of orientation error respectively. Figure 4 shows the end-effector trajectory performed on the *unknown* planar surface in the image frame and robot frame.

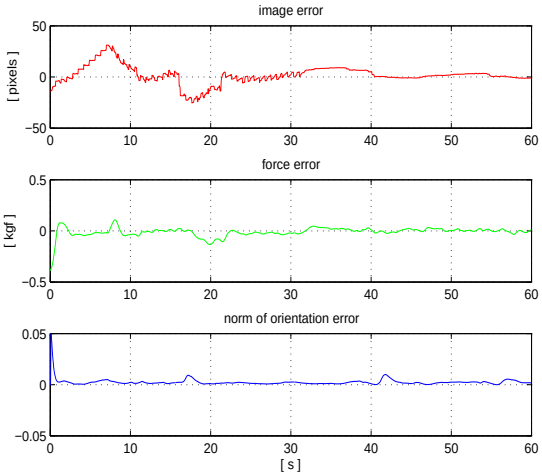

Figure 3: Image error, force error and norm of orientation error.

8 Conclusion

This work has proposed a hybrid vision and force control method for the visual tracking of a desired trajectory, while keeping the end-effector tip in orthogonal contact with a smooth surface and exerting a prescribed contact force. The camera parameters as well as the surface geometry is supposed to be uncertain.

Adaptive visual servoing is proposed to cope with the camera uncertainties and the reorientation scheme for the end-effector is devised based on direct force measurements, taking into account possible friction force due to the contact with the surface. The stability analysis of the overall control system was presented. Simulation and experimental results show the applicability of the proposed control scheme.

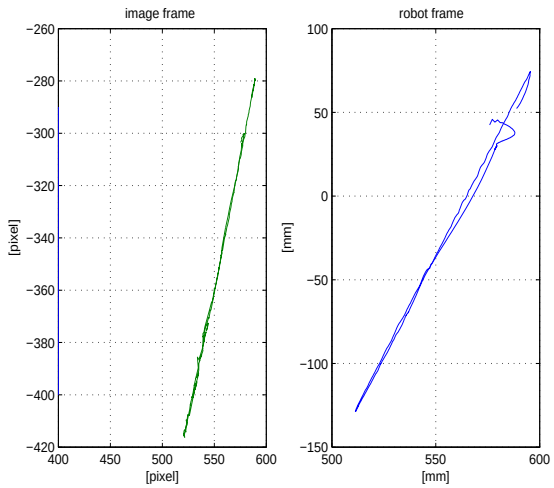

Figure 4: End-effector trajectory in the image frame and robot frame.

Future research topic following the ideas developed here is to relax the complete knowledge of the robot kinematics and to include the effects of the nonlinearity and uncertainty in robot dynamics.

References

[1] K. Hosoda, K. Igarashi and M. Asada, "Adaptive hybrid control for visual and force servoing in unknown environment", *IEEE Robotics and Automation Magazine*, pp. 39–43, 1998.

[2] A. Pichler and M. Jagersand, "Uncalibrated hybrid force-vision manipulation", *IEEE Conf. on Intelligent Robots and Systems*, vol. 3, pp. 1866–1871, 2000.

[3] J. Baeten and J. D. Schutter, "Hybrid vision/force control at corners in planar robotic-contour following", *ASME Trans. on Mechatronics*, vol. 7, no. 2, pp. 143–150, 2002.

[4] Y. Zhao and C. C. Cheah, "Hybrid vision-force control for robot with uncertainties", *IEEE Int. Conf. on Robotics & Automation*, pp. 261–266, 2004.

[5] T. Yoshikawa and A. Sudou, "Dynamic hybrid position/force control of robot manipulators – online estimation of unknown constraint", *IEEE Trans. on Control Systems Technology*, vol. 9, no. 2, pp. 220–226, 1993.

[6] R. M. Murray, Z. Li and S. S. Sastry, *A Mathematical Introduction to Robotic Manipulation*, CRC Press, 1996.

[7] A. C. Leite, F. Lizarralde and L. Hsu, "Hybrid vision-force robot control for tasks on unknown smooth surfaces", *IEEE Int. Conf. on Robotics & Automation*, 2006.

[8] F. Lizarralde and J. T. Wen, "Attitude control without angular velocity measurements: a passivity approach", *IEEE Trans. on Automatic Control*, vol. 41, no. 3, pp. 1–5, 1995.

[9] H. K. Khalil, *Nonlinear Systems*, Prentice Hall, 3rd Ed., 1996.

[10] M. Mason, "Compliance and force control for computer controlled manipulators", *IEEE Trans. on Systems, Man and Cybernetics*, vol. 11, no. 6, pp. 418–432, 1981.

[11] S. Hutchinson, G. Hager and P. Corke, "A tutorial on visual servo control", *IEEE Trans. Robotics and Automation*, vol. 12, no. 5, pp. 651–670, 1996.

[12] L. Hsu and P. Aquino, "Adaptive visual tracking with uncertain manipulator dynamic and uncalibrated camera", *IEEE Conf. on Decision and Control*, pp. 1248–1253, 1999.

[13] R. R. Costa, L. Hsu, A. K. Imai and P. Kokotovic, "Lyapunov-based adaptive control of MIMO systems", *Automatica*, vol. 39, no. 5, pp. 1251–1257, 2003.

[14] E. Zergeroglu, D. Dawson, M. de Queiroz and S. Nagarkatti, "Robust visual-servo control of robot manipulators in the presence of uncertainty", *IEEE Conf. on Decision and Control*, pp. 4137–4142, 1999.